Electro-osmotic flows of viscoelastic fluids: a numerical study

A.M. Afonso[1], F. T. Pinho[2] and M. A. Alves[1]

[1] Departamento de Engenharia Química, CEFT, Faculdade de Engenharia da Universidade do Porto, Rua Dr. Roberto Frias, 4200-465 Porto, Portugal.
email: {aafonso, mmalves}@fe.up.pt, http://www.fe.up.pt/~ceft
[2] Departamento de Engenharia Mecânica, CEFT, Faculdade de Engenharia da Universidade do Porto, Rua Dr. Roberto Frias, 4200-465 Porto, Portugal.
email: fpinho@fe.up.pt, http://www.fe.up.pt/~ceft

Summary

In this work we present a finite volume method (FVM) used to solve the relevant coupled equations for electro-osmotic flows (EOF) of viscoelastic fluids, using the Upper-Convected Maxwell (UCM) and the simplified Phan-Thien—Tanner (sPTT) models. Studies were undertaken in the cross-slot geometry, to investigate the possible appearance of purely-elastic instabilities, by considering the effect of the electric field. We found that even for pure electro-osmotic flow, i.e., in absence of an imposed pressure gradient, we were able to capture the onset of an asymmetric flow above a critical Deborah number, which is lower than the corresponding value for pressure gradient forcing.

Keywords: *Electro-osmosis, cross-slot flow, UCM model, PTT fluid, Finite-Volume Method.*

1 Introduction

Accurate flow control in microfluidic devices requires techniques that can easily be miniaturized and an obvious candidate is electrokinetic forcing through such mechanisms as electro-osmosis or electrophoresis. An overview of these and other electrokinetic techniques can be found in Bruus [1].

Electro-osmosis is an electrokinetic phenomenon, first demonstrated by Reuss [2] early in the 19th century, where the channel flow of a polar fluid is forced by an external electric field applied between the inlet and outlet and acting on ions existing near the channel walls. Helmholtz [3] proposed the electric double layer (EDL) theory that relates the electrical and flow parameters for electrokinetic transport in 1879. Subsequently, Smoluchowski [4] generalized Helmholtz's double layer theory by taking into account the actual charge/ potential distributions in a capillary channel. A more realistic concept of these distributions in the fluid adjacent to the capillary wall was introduced by Gouy [5] in 1910. Debye and Hückel [6] determined the ionic number concentration in a solution of low ionic energy, by means of a linearization of the exponential Boltzmann ion energy distribution. For Newtonian fluids, rigorous modeling of the electro-osmotic flow in microchannels has been the subject of several studies [7-10], and a thorough review on various other aspects of electro-osmosis can be found in Karniadakis et al [11]. The theoretical study of electro-osmotic flows of non-Newtonian fluids is recent and most works have been limited to simple inelastic fluid models, such as the power-law, due to the inherent analytical difficulties introduced by more complex constitutive equations [12-15]. Recently these studies were extended to viscoelastic fluids by Afonso et al [16], who presented analytical solutions for channel and pipe flows of viscoelastic fluids under the mixed influence of electrokinetic and pressure forces, using two constitutive models: the simplified Phan-Thien—Tanner model (sPTT) [17], with linear kernel for the stress coefficient function and zero second normal stress difference [18], and the FENE-P model, based on the kinetic theory for Finitely Extensible Non-linear Elastic dumbbells with a Peterlin approximation for the average spring force (cf. Bird et al [19]). Their analysis [16] was restricted to cases with small electric double-layers, where the distance between the walls of a microfluidic device is at least one order of magnitude larger than the EDL, and the fluid had a uniform distribution across the channel. When the viscoelastic flow is induced by a combination of both electric and pressure potentials, in addition to the single contributions from these two mechanisms, there is an extra term in the velocity profile that simultaneously combines both forcings, which is absent for the Newtonian fluids where the superposition principle applies. This extra term contributes significantly to the total flow rate, depending on the value of the relative microchannel ratio, and appears only when the rheological constitutive equation is non-linear. Afonso et al [20] extended this study to the flow of viscoelastic fluids under asymmetric zeta potential forcing.

In the recent years the efforts for numerical modeling and simulation of EOF has also increased, especially when applied to Newtonian fluids. Yang and Li [21] developed a numerical algorithm for elecrokinetically driven

Newtonian liquid flows, using the Debye-Hückel approximation [6]. The same approximation was used by Patankar and Hu [22] in the numerical simulation of microfluidic injection of Newtonian fluids, with electro-osmotic forces through the intersection of two channels. Ermakov et al [23] developed a finite difference method (FDM) for electro-osmotic and electrophoretic transport and species diffusion for two-dimensional complex geometry flows of Newtonian fluids. Using the Gouy-Chapman approximation [5], Bianchi et al [24] developed a finite-element method (FEM) to study electro-osmotically driven microflows of Newtonian fluids in T-junctions. Dutta et al [25] used a spectral element method (SEM) for solution of the Poisson–Boltzmann and incompressible Navier–Stokes equations, to analyze mixed electro-osmotic/pressure driven flows of Newtonian fluids in two-dimensional geometries, such as straight channels and T-junction geometry. The previous work was later extended to complex microgeometries (cross-flow and Y-split junctions) by Dutta et al [26]. Lin et al [27] solved the Nernst–Planck and the full Navier–Stokes equations using FDM to model the EOF of Newtonian fluids in microfluidic focusing chips.

For non-Newtonian fluids the efforts for numerical modeling of EOF are now gathering momentum, with limited advance having been made, still for very simple geometries such as straight microchannels. Recently, Park and Lee [28] calculated numerically the electro-osmotic velocity of viscoelastic fluids in a square microchannel with and without externally imposed pressure gradient, using a generalized constitutive equation, which encompasses the upper-convected Maxwell (UCM) model, the Oldroyd-B model and the PTT model. Very recently, Tang et al [29], presented a numerical study of EOF in microchannels of non-Newtonian purely viscous fluids described by the power law model, using the lattice Boltzmann method. Zimmerman et al [30] presented two-dimensional FEM simulations of EOF in a microchannel T-junction of a purely viscous fluid described by a Carreau-type nonlinear viscosity. The motion within the electrical double layer at the channel walls was approximated by velocity wall slip boundary conditions.

In this work, and for the first time to our best knowledge, we perform numerical EOF simulations of viscoelastic fluids in more complex geometries. We use an FVM to solve the relevant coupled equations for electro-osmotic flows of viscoelastic fluids, namely the nonlinear Poisson– Nernst–Planck equation that governs the electrical double-layer field, the Cauchy equation with a body force due to the applied electrical potential field and a variety of constitutive equations for the viscoelastic fluids, in particular the UCM and sPTT models. In addition to the simulations in a complex geometry (Cross-Slot geometry), and in order to test the implementation of the numerical method, some predictions are compared with existing analytical solutions for the flow in a two-dimensional microchannel under symmetric and asymmetric boundary conditions for the zeta potential at the walls [16,20].

The remaining of the paper is organized as follows: in sections 2 and 3 we briefly present the governing equations and outline the numerical method used to simulate the EOF of the viscoelastic fluids, respectively. In section 4, the main results of the numerical implementation tests and of the EOF in a cross-slot geometry are presented, respectively. A summary of the main findings closes the paper in section 5.

2 Governing equations

The flow is assumed to be steady, laminar and the fluid is incompressible. The governing equations describing the flow are the continuity equation,

$$\nabla \cdot \mathbf{u} = 0 \tag{1}$$

and the Cauchy equation:

$$\rho\left[\frac{\partial \mathbf{u}}{\partial t} + \nabla \cdot \mathbf{uu}\right] = -\nabla p + \beta\eta_0 \nabla^2 \mathbf{u} + \frac{\eta_0}{\lambda}(1-\beta)\nabla \cdot \mathbf{A} + \mathbf{F} \tag{2}$$

where $\mathbf{u}$ is the velocity vector, p the pressure, t the time, ρ the fluid density, η_s the Newtonian solvent viscosity and $\mathbf{A}$ is the conformation tensor. The polymer solution either obeys the UCM or the sPTT models, hence the total fluid extra stress is the sum of the solvent and polymer stress contributions. The equations are written in general form. The polymer has a relaxation time λ and a viscosity coefficient η_p, defining a zero-shear rate total viscosity $\eta_0 = \eta_p + \eta_s$. The coefficient β in equation (2) is the ratio between the solvent viscosity and η_0 ($\beta = \eta_s/\eta_0$) and is a measure of the concentration of polymer additive ($\beta = 0$ implies no solvent and $\beta = 1$ means that the fluid is Newtonian and there is no polymer additive).

The polymer extra-stress $\boldsymbol{\tau}$ can be related to the conformation tensor $\mathbf{A}$ using

$$\boldsymbol{\tau} = \frac{\eta}{\lambda}(\mathbf{A} - \mathbf{I}) \tag{3}$$

which requires the solution of an evolution equation of the form,

$$\lambda\left[\frac{\partial \mathbf{A}}{\partial t} + \nabla \cdot \mathbf{uA}\right] + Y(\mathrm{tr}\mathbf{A})\mathbf{A} = Y(\mathrm{tr}\mathbf{A})\mathbf{I} + \lambda\left(\mathbf{A} \cdot \nabla \mathbf{u} + \nabla \mathbf{u}^T \cdot \mathbf{A}\right) \tag{4}$$

where **I** is the unitary tensor. When $Y(\text{tr}\,\mathbf{A})=1$ we recover the Oldroyd-B model which further simplifies to the UCM equation if $\beta = 0$. Otherwise, we are in the presence of the sPTT model with a Newtonian solvent and $Y(\text{tr}\,\mathbf{A})$ imparts to the fluid shear-thinning behavior and bounds the extensional viscosity as explained in the original papers of Phan-Thien and Tanner [17] and Phan-Thien [18].
In its general form function $Y(\text{tr}\mathbf{A})$ is exponential, but in this work we use its linear form

$$Y\left(tr\mathbf{A}\right) = 1 + \varepsilon\left(tr\mathbf{A} - 3\right) \tag{5}$$

The **F** term in the Cauchy equation (2) represents a body force per unit volume, given as

$$\mathbf{F} = \rho_e \mathbf{E} \tag{6}$$

where **E** is the applied external electric field and ρ_e is the net electric charge density. The electric field intensity is related to the electric potential, Φ, by

$$\mathbf{E} = -\nabla\Phi \tag{7}$$

while the electric potential is governed by,

$$\nabla^2\Phi = -\frac{\rho_e}{\in} \tag{8}$$

where $\in$ is the electrical permittivity of the solution. Two types of electric fields can be identified in EOF flows, depending on their origin. One is the applied electric field generated by the electrodes at the inlet and the outlet of the flow geometry, ϕ. The other electric field is due to the net charge distribution in the EDL, due to the charge acquired at the wall ψ. The total electric field is simply a linear superposition of these two contributions, and this can be written as

$$\Phi = \phi + \psi \tag{9}$$

Consequently, equation (8) can be rewritten as two separate equations,

$$\nabla^2\phi = 0 \tag{10}$$

and

$$\nabla^2\psi = -\frac{\rho_e}{\in} \tag{11}$$

Finally, we need to quantify the electric charge density in order to have a closed-form equation. For a symmetric electrolyte the ions and the counter-ions have the same charge valence, $z^+ = -z^- = z$, and the net electric charge density is given by:

$$\rho_e = ez\left(n^+ - n^-\right) \tag{12}$$

where n^+ and n^- are the concentrations of the positive and negative ions, respectively, and e is the elementary electric charge. In order to find the net charge density ρ_e, the distributions of ionic concentrations n^+ and n^- must be determined. This is achieved by solving the following transport equation, known as the Nernst-Planck equations:

$$\frac{\partial n^{\pm}}{\partial t} + \mathbf{u}\cdot\nabla n^{\pm} = \nabla\cdot\left(D^{\pm}\nabla n^{\pm}\right) \pm \nabla\cdot\left[D^{\pm}n^{\pm}\frac{ze}{k_B T}\nabla\left(\phi+\psi\right)\right] \tag{13}$$

where D^+ and D^- are the diffusion coefficients of the positive and negative ions, respectively. The set of equations (10) to (13) is usually called the Poisson-Nernst-Planck equations (PNP).

Another way to quantify the electric charge density is using the widely adopted Poisson–Boltzmann equation derived from the Nernst–Planck equations. From the ionic transport equations (13), when the ionic distribution is stationary, the electric double layer does not overlap at the center of the channel and significant variations of $n^{\pm}$ and ψ occur only in the normal direction to the channel walls, the stable Boltzmann distribution of ions in the electric double layer can be assumed, that according to Bruus [1] is given by

$$\rho_e = -2n_o ez\sinh\left(\frac{ez}{k_B T}\psi\right) \tag{14}$$

where $n_o = CN_A$ is the bulk number concentration of ions in the electrolyte solution, C is the molar concentration of ions, N_A is Avogadro's number, T is the temperature and k_B is the Boltzmann constant. The set of equations (10), (11) and (14) is usually called the Poisson- Boltzmann equations (PB).

For small values of $ez\zeta_o/k_B T$, synonymous of a small ratio of electrical to thermal energies, equation (14) can also be linearized, $\sinh(x) \approx x$, using the so-called Debye-Hückel approximation. Then, the electric charge density equation, becomes

$$\rho_e = -\in \kappa^2\psi \tag{15}$$

where $\kappa^2 = 2n_o e^2 z^2/(\in k_B T)$ is the Debye-Hückel parameter, related to the thickness of the Debye layer, $\lambda_D = 1/\kappa$ (also referred to as the EDL thickness). The set of equations (10), (11) and (15) is usually called the Poisson-Boltzmann-Debye-Hückel equations (PBDH).
Finally, we can rewrite the Cauchy equation (2) as,

$$\rho\left[\frac{\partial \mathbf{u}}{\partial t} + \nabla\cdot\mathbf{uu}\right] = -\nabla p + \beta\eta_0\nabla^2\mathbf{u} + \frac{\eta_0}{\lambda}(1-\beta)\nabla\cdot\mathbf{A} - \rho_e\nabla(\phi+\psi) \tag{16}$$

keeping in mind that the electric charge density equation can be obtained by equations (12), (14) or (15), depending on the desired level of approximation.

3 Numerical method

In the past, our group adapted a Newtonian FVM to calculate pressure driven flows of viscoelastic fluids. The method is based on a time marching pressure-correction algorithm formulated with the collocated variable arrangement and is explained in detail in Oliveira et al [31] and Alves et al [32]. For improved convergence, the FVM was modified with the matrix logarithmic of the conformation tensor [33], and details of that implementation have been previously given by Afonso et al [34].

Here, the existing method was extended to mixed electro-osmotic/pressure driven flows, and the modifications are explained below. As observed in the previous section, the new set of equations depends on the approximations applied to the closed-form equation for the electric charge density, i.e., the PNP, PB or PBDH equations. This fact also reflects on the numeric implementation, and we chose to implement all the three approximations. Briefly, the PNP, PB or PBDH equations are transformed first to a non-orthogonal system (ξ_l), but keeping the Cartesian velocity and stress components. This is advantageous from a numerical point of view, because the equations are written in a strong conservation form which helps to ensure that the final algebraic equations retain conservativeness. Then, the equations are integrated in space over the control volumes (cells with volume V_p) forming the computational mesh, and in time over a time step (δt), so that sets of linearised algebraic equations are obtained, having the general form:

$$a_P^\Theta \Theta_P = \sum_{F=1}^{6} a_F^\Theta \Theta_F + S^\Theta \tag{17}$$

to be solved for all variables (Θ=u, v, w, ϕ, ψ, n^+ or n^-). The equations for the pressure and extra stress components (or the Log-conformation tensor) are similar to equation (17) and are the same used in the pressure driven flow version of the code (see [31-32]), and so they are not included in this description. In these equations a_F are coefficients accounting for convection and diffusion, S^Θ are source terms encompassing all contributions not included in the coefficients, the subscript P denotes the cell under consideration and subscript F its corresponding neighbouring cells. The coefficients of the PNP equations are given by:

$$\begin{cases} a_F^\phi = D_f; \qquad a_P^\phi = \sum_{F=1}^{6} a_F^\phi; \qquad S^\phi = 0 \\ a_F^\psi = D_f; \qquad a_P^\psi = \sum_{F=1}^{6} a_F^\psi; \qquad S^\psi = \dfrac{ez}{\in}\left(n^+ - n^-\right)V_P \\ a_F^{n^\pm} = D_f + C_f; a_P^{n^\pm} = \dfrac{V_P}{\delta t} + \sum_{F=1}^{6} a_F^{n^\pm}; S^{n^\pm} = S_{HRS}^{n^\pm} + \left[\dfrac{n^\pm}{\delta t} \pm \left(\dfrac{D^\pm n^\pm}{2}\kappa^2\left(n^- - n^+\right) + \sum_{i=1}^{3}\dfrac{\partial\left(D^\pm n^\pm \dfrac{ze}{k_B T}\right)}{\partial x_i}\dfrac{\partial(\phi+\psi)}{\partial x_i}\right)\right]V_P \\ S_E^{uvw} = ez\left(n^+ - n^-\right)\nabla(\phi+\psi)V_P \end{cases} \tag{18}$$

where D_f and C_f are the diffusive and convective conductance, respectively. The term S_E^{uvw} is the electric body force term in the momentum equations (16), and is added to the other source terms in the momentum equation (see [31-32]). The coefficients of the PB equations are given by:

$$\begin{cases} a_F^{\phi} = D_f; \qquad a_P^{\phi} = \sum_{F=1}^{6} a_F^{\phi}; \qquad S^{\phi} = 0 \\ a_F^{\psi} = D_f; a_P^{\psi} = \sum_{F=1}^{6} a_F^{\psi} + \kappa^2 \cosh\left(\frac{ez}{k_B T}\psi\right) V_P; S^{\psi} = \left[\kappa^2 \psi \cosh\left(\frac{ez}{k_B T}\psi\right) - 2\frac{n_o ez}{\in} \sinh\left(\frac{ez}{k_B T}\psi\right)\right] V_P \\ S_E^{uvw} = 2 n_o ez \sinh\left(\frac{ez}{k_B T}\psi\right) \nabla(\phi + \psi) V_P \end{cases} \tag{19}$$

In the coefficients for the potential ψ, especial attention was given to the hyperbolic function $\sinh(ez\psi/k_BT)$, especially at high values of $ez\psi/k_BT$, due to the exponential behavior of the function. So, a linearization of the source term, S^{ψ} was introduced in equation (19). Finally, the coefficients of the PBDH equations are given by:

$$\begin{cases} a_F^{\phi} = D_f; \qquad a_P^{\phi} = \sum_{F=1}^{6} a_F^{\phi}; \qquad S^{\phi} = 0 \\ a_F^{\psi} = D_f; \qquad a_P^{\psi} = \sum_{F=1}^{6} a_F^{\psi} + \kappa^2 V_P; \qquad S^{\psi} = 0 \\ S_E^{uvw} = \in \kappa^2 \psi \nabla(\phi + \psi) V_P \end{cases} \tag{20}$$

The CUBISTA high-resolution scheme [32] was used in the discretization of the convective terms of the momentum, of the Log-conformation tensor and of the ionic transport equations (13) (see term $S_{HRS}^{n^{\pm}}$ in equations (18)). This scheme is formally of third-order accuracy and was especially designed for differential constitutive relations (see [32]). Due to the lack of space and because we will use small EDL thickness (and so the electric double layer does not overlap at the center of the channels), and we also assume that significant variations of $n^{\pm}$ and ψ occur only in the normal direction to the channel walls, then only the PB version of the code is used in the present work.

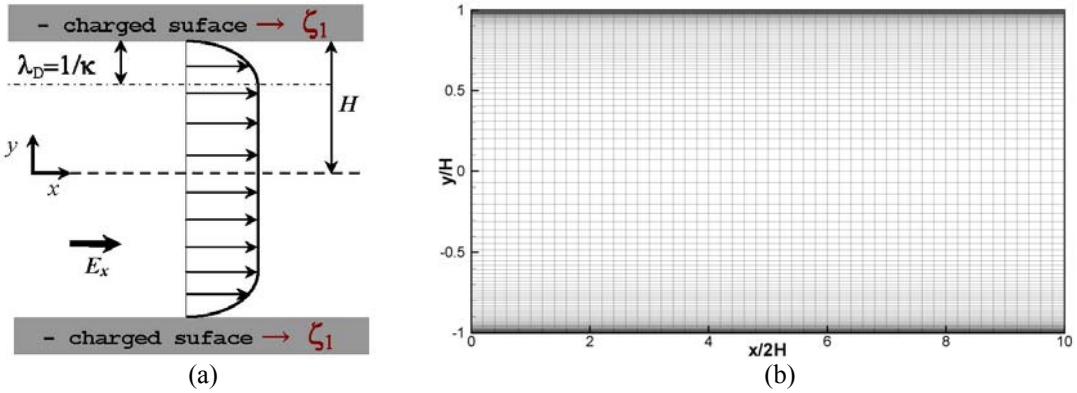

(a) (b)

Fig.1. (a) Channel geometry and (b) mesh M3.

4 Results and discussion

4.1 Accuracy tests

To test the implementation of the numerical method some predictions are compared with existing analytical solutions for the flow in a two-dimensional microchannel under symmetric and asymmetric boundary conditions for the zeta potential at the walls [16,20]. In those works the so-called standard electrokinetic model assumptions were used, along with the sPTT model for the viscoelastic fluid. When the flow is fully-developed the velocity and stress fields only depend on the transverse coordinate y, and on some dimensionless parameters, such as the ratio of microchannel to Debye layer thicknesses $\bar{\kappa} = \kappa H$, the Helmholtz-Smoluchowski electro-osmotic velocity $u_{sh} = -\in \zeta_i E_x / \eta$, the rheological properties of the fluid via a Deborah number based on the EDL thickness and u_{sh}, $De_k = \lambda u_{sh} / \lambda_D = \lambda \kappa u_{sh}$ (or based in the channel length, $De_H = \lambda u_{sh} / H$ as in [16]) and the fluid extensibility parameter ε. To account for the combined forcing of pressure gradient and electro-osmosis, the non-dimensional ratio between these two forcings is given by $\Gamma = -\left(H^2 / \in \zeta_i\right)\left(p_{,x} / E_x\right)$.

Table 1. Mesh details.

	NC	Δx_{min}	Δy_{min}
M1	1800	0.2	$8.0\text{x}10^{-4}$
M2	3600	0.2	$4.0\text{x}10^{-4}$
M3	7200	0.2	$2.0\text{x}10^{-4}$
MCS	12801	$4.0\text{x}10^{-4}$	$4.0\text{x}10^{-4}$

The channel geometry is represented in **Figure 1(a)**. At the walls the no-slip condition applies ($u = 0$ at $y = \pm H$), along with $\partial\phi/\partial y|_{wall} = 0$ and $\psi = \zeta_i$. Depending on the value of ζ_i on the walls, we can determine if the flow is symmetric ($R_\zeta = \zeta_1/\zeta_2 = 1$, i.e. $\zeta_1 = \zeta_2$) or asymmetric ($R_\zeta = \zeta_1/\zeta_2 \neq 1$, i.e. $\zeta_1 \neq \zeta_2$). At the inlets fully-developed velocity and stress profiles are imposed and at the outlet planes Neumann boundary conditions are applied, i.e. $\partial\theta/\partial x = 0$).

The main characteristics of the three meshes used in this work for the accuracy test are given in **Table I**, including the total number of cells (NC) and the minimum cell spacing ($\Delta x_{\min}$ and $\Delta y_{\min}$). Note that the refinement in the transverse direction is very high, in order to obtain accurate results in the sharp zone of the EDL. This high refinement is shown in **Figure 1(b)**, here for mesh M3.

The results for the accuracy tests are presented in **Figure 2**. When $R_\zeta = 1$, i.e., for symmetric conditions, **Figure 2(a)**, presents the fully-developed dimensionless velocity profiles obtained with $\varepsilon = 0.25$, $De_k = 1$, $\bar{\kappa} = 200$ and $\Gamma = 0$ (pure EOF). As observed, both the analytical and numerical results collapse, showing excellent accuracy, even at a very sharp EDL ($\bar{\kappa} = 200$). For complete asymmetric flow ($R_\zeta = -1$), with $\varepsilon = 0.25$, $De_k = 1$, $\bar{\kappa} = 50$ and in the presence of a favourable pressure gradient (with $\Gamma = -2$), the comparison between the analytical and numeric results is also excellent, as observed in **Figure 2(b)**. These results show that the refinement near the wall for mesh M2 is sufficient to obtain accurate results, even for very small EDL thickness.

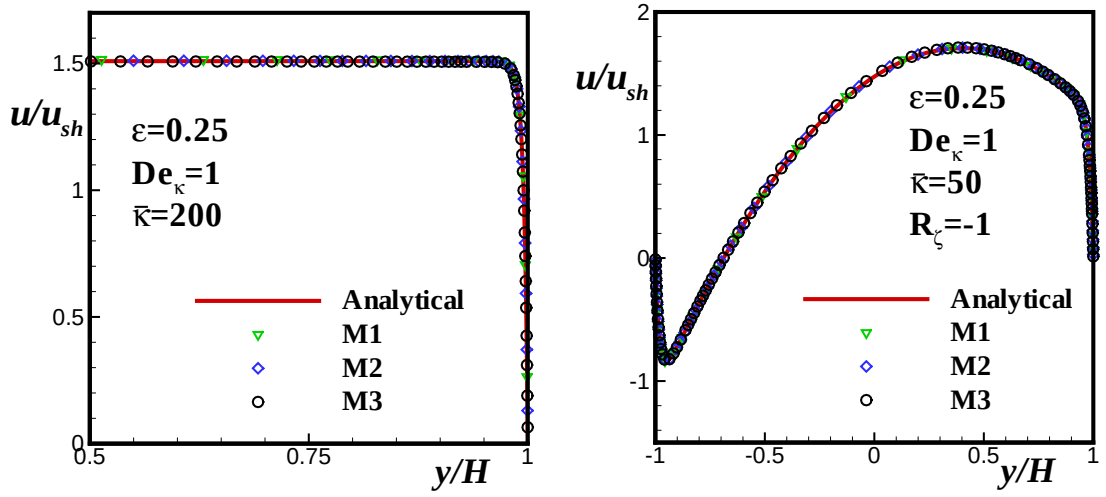

Fig.2. Dimensionless velocity profiles for (a) symmetric zeta potential for pure EOF ($\Gamma = 0$) and (b) asymmetric zeta potential for favourable pressure gradient ($\Gamma = -2$)

4.2 Cross-Slot flow results

Further studies were undertaken in a more complex geometry, usually described as cross-slot geometry (see **Figure 3**). We are particularly interested in investigating the possible appearance of purely-elastic instabilities, as observed recently in a three-dimensional cross-slot microchannel flow by Arratia et al [35], under pure Poiseuille flow. Poole et al [36] simulated the two-dimensional cross-slot flow of an UCM fluid under creeping-flow conditions, and were able to capture qualitatively the onset of a bistable steady asymmetric flow above a first critical Deborah number followed by a later transition to a time dependent flow, in agreement with the experimental findings of Arratia et al [35]. Poole at al [37] extended the earlier study of Ref. [36] by considering the three-dimensional nature of a real microfluidic cross slot flow and investigated in detail the effect of the aspect ratio of the geometry, by varying the depth of the cross slot from low values (quasi-Hele Shaw flow) up to very large values (quasi-two dimensional flow). Later, Poole et al [38] incorporated the effect of solvent viscosity ($\beta \neq 0$ in the Oldroyd-B) and finite extensibility ($\varepsilon \neq 0$ in the sPTT model), presenting some β-Re-De and ε-Re-De maps of flow pattern types, showing the existence of a narrow region where steady asymmetric flow can emerge, and identified the limiting De for onset of time-dependent flow. The effect of finite

extensibility was also studied by Rocha et al [39], using FENE models. Afonso et al [40] presented a numerical study of the creeping flow of an UCM fluid in a three-dimensional cross-slot geometry with six arms and studied the influence of the different types of extensional flow near the stagnation point. They found that the uniaxial extension flow configuration is prone to the onset of steady flow asymmetries, while in the biaxial extension flow configuration the flow was perfectly symmetric.

In this work we further extend the previous investigations by considering the effect of the electric field in the appearance of the flow instabilities. The cross-slot geometry is shown schematically in **Figure 3** together with the mesh used in this work. All branches have the same width (H) and the inlet and outlet branches have lengths of twenty channel widths ($20H$). At the inlets fully-developed velocity and stress profiles are imposed and the inlet length is more than sufficient for the flow at the junction to be independent of the inlet condition. Similarly, the outlets are sufficiently long to avoid any effect of the outflow boundary condition upon the flow in the central region. At the outlet planes vanishing axial gradients are applied to all variables (Neumann boundary conditions, i.e. $\partial\varphi/\partial y = 0$), and no-slip conditions are imposed at all channel walls. For the potential at the walls, we assume $\partial\phi/\partial n|_{wall} = 0$ and $\psi = \zeta_i$. The mesh used in these calculations has the same refinement near the walls as mesh M2 of the accuracy tests, and the main characteristics of that mesh are also given in **Table I**. Near the central square, and as observed in **Figure 3(b)**, the mesh in the axial direction is also very refined, with both minimum cell spacings equal $\Delta x_{min} = \Delta y_{min} = 4.0\times10^{-4}$. All the calculations were carried out at a vanishing Reynolds number, $Re = \rho UH/\eta = 0$ (creeping flow conditions – imposed by dropping out the convective term in the momentum equation).

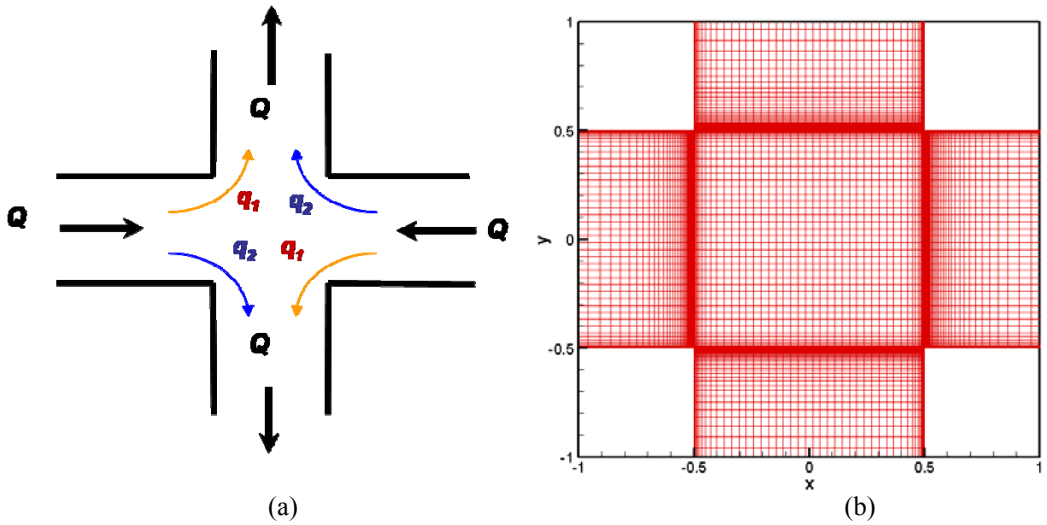

(a) (b)

Fig.3. (a) Cross-slot geometry and (b) mesh MCS.

As already described, we are particularly interested in the effect of the electric field in the possible appearance of asymmetries in the cross-slot flow. We start presenting the effect of the combined forcing by pressure gradient and electro-osmosis in the flow characteristics. Theoretically, for Newtonian fluid flow in a straight channel, when the non-dimensional ratio between these two forcings is $\Gamma = 2$, the dimensionless velocity at the center line is zero (due to the adverse effect of both forcing terms, i.e., pressure is driving the flow in one direction while electric potential drives it in the opposite direction). **Figure 4(a)**, shows the streamlines superimposed with the u-velocity contours for this situation. We can observe that near the walls the EOF is driving the flow towards the central square while in the center line of the channel the backpressure drives the flow out in the channel. This is also evident if the adverse pressure gradient is increased, as observed in **Figure 4(b)**, here for $\Gamma \approx 2.5$.

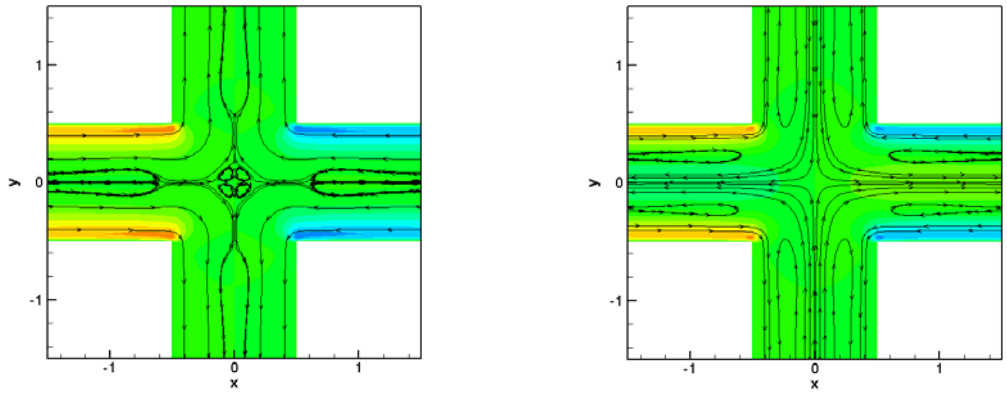

(a) (b)

Fig.4 Streamlines superimposed over axial velocity field for Newtonian flow for adverse pressure gradients: (a) $\Gamma \approx 2$ and (b) $\Gamma \approx 2.5$.

For viscoelastic fluids we performed additional simulations with $\Gamma \approx 0$, i.e., for pure EOF, and $\bar{\kappa} = 20$ using the UCM model. **Figure 5** presents the streamlines superimposed over *u*-velocity contour maps for UCM flow for several Deborah numbers, showing that above a critical Deborah number ($De_H \geq 0.275$) the flow becomes asymmetric. The differences between the results for the cross slot with pure EOF and pure pressure gradient flows may be understood from the role of the amount of stabilizing shear flow in the stagnation point region which is less in the case of EOF. This difference may also be important for understanding the appearance of the purely-elastic instabilities in the cross slot geometry. At higher Deborah numbers the flow becomes unsteady, with the formation of vortical structures in the central square, but these flow conditions require further studies, to be undertaken in the future.

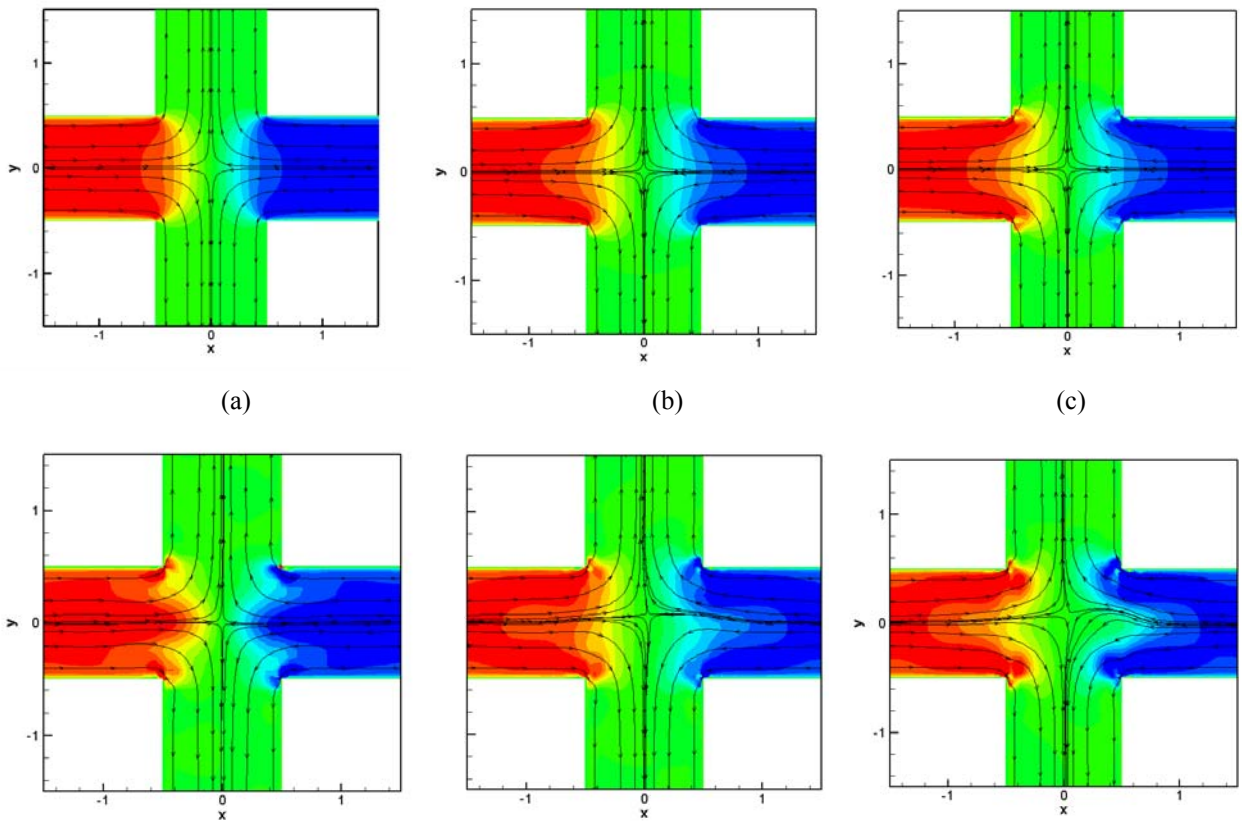

(a) (b) (c)

(d) (e) (f)

Fig.5 Streamlines superimposed over *u*-velocity field for pure EO flow of UCM fluid: (a) steady symmetric flow at De_H =0; (b) De_H =0.1, (c) De_H =0.2; (d) De_H =0.25 and steady asymmetric flow at (e) De_H =0.275 and (f) De_H =0.3.

5 Conclusions

In this work we present a finite volume method that can be used to solve the relevant coupled equations for electro-osmotic flows of viscoelastic fluids, namely the nonlinear Poisson–Boltzmann equation that governs the electrical double-layer field, the Cauchy equation with a body force due to the applied electrical potential field and the constitutive equations for the viscoelastic fluids.

To describe the rheological behavior of viscoelastic fluids we use the Upper-Convected Maxwell (UCM) model and the simplified Phan-Thien—Tanner model (sPTT) [17]. We tested the implementation of the numerical method against existing analytical solutions for the flow in a two-dimensional microchannel under symmetric

and asymmetric boundary conditions for the zeta potential at the walls [16,20], and the comparison between the analytical and numeric results collapsed within numerical uncertainty, even for very small EDL thickness.

In this work we further extend the previous investigations in the cross-slot geometry by considering the effect of the electric field in the appearance of the flow instabilities, and found that even for pure electro-osmotic flow (in absence of any imposed pressure gradient) we were able to capture the onset of an asymmetric steady flow above a critical Deborah number, De_H =0.275, which was lower than for pure pressure gradient forcing.

Acknowledgments

The authors are grateful to FCT for funding this work through grants number PTDC/EME-MFE/70186/2006 and PTDC/EQU-FTT/71800/2006. A. M. Afonso would also like to thank FCT for financial support through the scholarship SFRH/BD28828/2006.

References

1. H. Bruus, *Theoretical Microfluidics*, Oxford Master Series in Condensed Matter Physics, Oxford University Press, Oxford, UK, 2008;
2. F.F. Reuss, Sur un nouvel effet de l'électricité galvanique, *Mémoires de la Societé Impériale dês Naturalistes de Moscou*, **2**, 327-337, 1809;
3. H. Helmholtz, Uber den einfluß der elektrischen grenzschichten bei galvanischer spannung und der durch wasserstromung erzeugten potentialdifferenz, *Ann.* **7**, 337, 1879;
4. M. von Smoluchowski, Versuch einer mathematischen theorie der kogulationskinetic kolloid losunaen, *Z. Phys. Chem.* **92**, 129–35, 1917;
5. G. Gouy, Sur la Constitution de la Charge Électrique à la Surface d'un Électrolyte, *J. Physiol* **9** 457-468 1910;
6. P. Debye and E. Hückel, Zur Theorie der Elektrolyte II. das Grenzgesetz für die elektrishe Leitfähigkeit, *Physik Z.* **24** 305-325 1923;
7. D. Burgreen and F.R. Nakache, Electrokinetic flow in ultrafine capillary slits. *J. Phys. Chem.*, **68**, 1084–1091, 1964;
8. C.L. Rice and R. Whitehead, Electrokinetic flow in a narrow cylindrical capillary. *J. Phys. Chem.*, **69**, 4017–4024, 1964;
9. S. Arulanandam and D. Li, Liquid transport in rectangular microchannels by electroosmotic pumping. *Colloids Surf. A.*, **161**, 29–102, 2000;
10. P. Dutta and A. Beskok, Analytical solution of combined electroosmotic/pressure driven flows in two-dimensional straight channels: Finite Debye Layer effects, *Anal. Chem.* **73**, 1979-1986, 2001;
11. G. Karniadakis, A. Beskok, N. Aluru, *Microflows and nanoflows. Fundamentals and Simulation.* Interdisciplinary Applied Mathematics Series, **29**, Spinger Verlag. 2005;
12. S. Das and S. Chakraborty, Analytical solutions for velocity, temperature and concentration distribution in electroosmotic microchannel flows of a non-Newtonian bio-fluid, *Analytica Chimica Acta* **559**, 15–24, 2006;
13. H.M. Park and W.M Lee, Helmholtz-Smoluchowski velocity for viscoelastic electroosmotic flows. *J. Colloid Interface Sci.* **317**, 631-636, 2008;
14. C.L.A. Berli and M.L. Olivares, Electrokinetic flow of non-Newtonian fluids in microchannels. *J. Colloid Interface Sci.* **320**, 582-589, 2008;
15. C. Zhao, E. Zholkovskij, J.H. Masliyah and C. Yang, Analysis of electroosmotic flow of power-law fluids in a slit microchannel, *J. Colloid Interface Sci.* **326,** 503–510, 2008;
16. A.M. Afonso, M.A. Alves and F.T. Pinho, Analytical solution of mixed electro-osmotic/pressure driven viscoelastic fluids in microchannels, *J. Non-Newt. Fluid Mech.*, **159**, 50-63, 2009;
17. N. Phan-Thien and R.I. Tanner, New constitutive equation derived from network theory, *J. Non-Newt. Fluid Mech.* **2**, 353–365, 1977;
18. N. Phan-Thien, A non-linear network viscoelastic model, *J. Rheol.* **22**, 259–283, 1978;
19. R.B. Bird, R.C. Armstrong, O. Hassager, *Dynamics of Polymeric Liquids*, vol. 1. Fluid Mechanics, 2nd ed., Wiley, New York, 1987;
20. A.M. Afonso, M.A. Alves and F.T. Pinho, Electro-osmotic flows of viscoelastic fluids in microchannels under asymmetric zeta potential, *in preparation*, 2009;

21. C. Yang and D. Li, Analysis of Electrokinetic Effects on the Liquid Flow in Rectangular Microchannels, *J. Colloids and Surfaces*, **143**, pp. 339-353, 1998;
22. N.A. Patankar and H.H. Hu, Numerical Simulation of Electroosmotic Flow, *Anal. Chem.*, **70**, 1870-1881, 1998;
23. S.V. Ermakov, S.C. Jacobson, and J.M. Ramsey, Computer Simulation of Electrokinetic Transport in Micro Fabricated Channel Structures, *Anal. Chem.*, **70**, 4494-4504, 1998;
24. F. Bianchi, R. Ferrigno, and H.H. Girault, Finite Element Simulation of an Electroosmotic-Driven Flow Division at a T-junction of Microscale Dimension, *Anal. Chem.*, **72**, 1987-1993, 2000;
25. P. Dutta, A. Beskok and T.C. Warburton, Numerical simulations of mixed electroosmotic/pressure driven microflows, *Numerical Heat Transfer, Part A*, **41**, 131-148, 2002;
26. P. Dutta, A. Beskok and T.C. Warburton, Electroosmotic Flow Control in Complex Microgeometries, *Journal of Microelectromechanical systems*, **11**, 1, 36-44, 2002;
27. J.Y. Lin, L.M. Fu and R.J. Yang, Numerical simulation of electrokinetic focusing in microfluidic chips, *J. Micromech. Microeng*. **12,** 955–961, 2002;
28. H.M. Park and W.M. Lee, Effect of viscoelasticity on the flow pattern and the volumetric flow rate in electroosmotic flows through a microchannel, *Lab Chip*, **8**, 1163–1170, 2008;
29. G.H. Tang, X.F. Li, Y.L. He and W.Q. Tao, Electroosmotic flow of non-Newtonian fluid in microchannels, *J. Non-Newt. Fluid Mech.* **157**, 133–137, 2009;
30. W.B. Zimmerman, J.M. Rees and T.J. Craven, Rheometry of non-Newtonian electrokinetic flow in a microchannel T-junction, *Microfluid Nanofluid,* **2**, 481–492, 2006;
31. P.J. Oliveira, F.T. Pinho and G.A. Pinto, Numerical simulation of non-linear elastic flows with a general collocated finite-volume method. *J. Non-Newt. Fluid Mech.*, **79**, 1-43, 1998;
32. M.A. Alves, P.J. Oliveira and F.T. Pinho, A convergent and universally bounded interpolation scheme for the treatment of advection, *International Journal for Numerical Methods in Fluids*, **41**, 47-75, 2003;
33. R. Fattal, R. Kupferman, Constitutive laws of the matrix-logarithm of the conformation tensor, *J. Non-Newt. Fluid Mech.* **123**, 281–285, 2004;
34. A. Afonso, P.J. Oliveira, F.T. Pinho, M.A. Alves, The log-conformation tensor approach in the finite-volume method framework, *J. Non-Newtonian Fluid Mech*. **157**, 55–65, 2009;
35. P.E. Arratia, C.C. Thomas, J.D. Diorio and J.P. Gollub. Elastic instabilities of polymer solutions in cross-channel flow. *Physical Review Letters*, **144502**, 2006;
36. R.J. Poole, M.A. Alves and P.J. Oliveira. Purely elastic flow asymmetries. *Physical Review Letters*, **99**, 164503, 2007;
37. R.J. Poole, M.A. Alves, A.M. Afonso, F.T. Pinho and P.J. Oliveira. Purely-elastic instabilities in a microfluidic cross-slot geometry. *AIChE 2007 Annual Meeting,* Salt Lake City, Paper 94827, 2007;
38. R.J. Poole, M.A. Alves, A.M. Afonso, F.T. Pinho and P.J. Oliveira. Purely elastic instabilities in a cross-slot flow. *The Society of Rheology 79th Annual Meeting,*Salt Lake City, 2007;
39. G.N. Rocha, R.J. Poole, M.A. Alves and P.J. Oliveira, On extensibility effects in the cross-slot flow bifurcation, *J. Non-Newt. Fluid Mech.* **156**, 58-69, 2009;
40. A.M, Afonso, M.A. Alves and F.T. Pinho. Purely elastic flow instabilities in a 3D six arms cross slot geometry. *Proceedings of the XVth International Congress of Rheology* (2008), Monterey, AIP Conference Proceedings Volume 1027, Paper 180_1, 2008.